Nonequilibrium dynamics and fluctuation-dissipation relation in a sheared fluid

Ludovic Berthier
CECAM, ENS-Lyon, 46, Allée d'Italie, 69007 Lyon, France

Jean-Louis Barrat
Département de Physique des Matériaux, UCB Lyon 1 and CNRS, 69622 Villeurbanne, France

(Received 11 October 2001; accepted 22 January 2002)

The nonequilibrium dynamics of a binary Lennard-Jones mixture in a simple shear flow is investigated by means of molecular dynamics simulations. The range of temperature T investigated covers both the liquid, supercooled, and glassy states, while the shear rate γ covers both the linear and nonlinear regimes of rheology. The results can be interpreted in the context of a nonequilibrium, schematic mode-coupling theory developed recently, which makes the theory applicable to a wide range of soft glassy materials. The behavior of the viscosity $\eta(T,\gamma)$ is first investigated. In the nonlinear regime, strong shear-thinning is obtained, $\eta \sim \dot{\gamma}^{-\alpha(T)}$, with $\alpha(T) \simeq \frac{2}{3}$ in the supercooled regime. Scaling properties of the intermediate scattering functions are studied. Standard ''mode-coupling properties'' of factorization and time superposition hold in this nonequilibrium situation. The fluctuation-dissipation relation is violated in the shear flow in a way very similar to that predicted theoretically, allowing for the definition of an effective temperature T_{eff} for the slow modes of the fluid. Temperature and shear rate dependencies of T_{eff} are studied using density fluctuations as an observable. The observable dependence of T_{eff} is also investigated. Many different observables are found to lead to the same value of T_{eff}, suggesting several experimental procedures to access T_{eff}. It is proposed that a tracer particle of large mass m_{tr} may play the role of an ''effective thermometer.'' When the Einstein frequency of the tracers becomes smaller than the inverse relaxation time of the fluid, a nonequilibrium equipartition theorem holds with $\langle m_{\mathrm{tr}} v_z^2 \rangle = k_B T_{\mathrm{eff}}$, where v_z is the velocity in the direction transverse to the flow. This last result gives strong support to the thermodynamic interpretation of T_{eff} and makes it experimentally accessible in a very direct way. © *2002 American Institute of Physics.* [DOI: 10.1063/1.1460862]

I. INTRODUCTION

Glasses are usually defined by the fact that their internal relaxation time is larger than the experimental time scale. In simple molecular systems, the associated glass transition temperature corresponds to a very high viscosity, making it difficult to investigate experimentally the rheological properties of glassy systems. In complex fluids (e.g., colloids, emulsions) it is, however, possible to reach a glassy situation, in the sense of large relaxation times, with systems having viscosities or shear moduli that allow for a rheological investigation.[1] Such materials have been described as ''soft glassy materials'' in the literature.[2]

When it is quenched into its glassy state, a material is by definition out of equilibrium. An important feature of this nonequilibrium situation is the absence of time translation invariance. Physical properties are a function of the time spent in the glassy phase, or waiting time t_w. This is best seen through the measurement of time-dependent correlations that depend both on t_w and on the time difference. These dependencies on t_w are usually described as aging phenomena.[3] They have been studied experimentally and theoretically in great detail.[4] Interestingly, for the present work, the aging behavior of several complex fluids has recently been experimentally investigated,[5–11] showing interesting similarities with other, more standard, glassy systems.

By submitting the system to a homogeneous, steady shear flow, a different kind of nonequilibrium situation is obtained. The steady shear flow, characterized by the shear rate γ, creates a *nonequilibrium steady state*, in which time translation invariance is recovered.[12] The shear flow can therefore be used as a probe of the glassy system, with the convenient feature of having the shear rate γ rather than the waiting time t_w as a control parameter. In fact, the inverse shear rate introduces a time scale in the problem, which plays a role similar to t_w. Interesting phenomena are thus expected to show up as soon as this new time scale competes with the relaxation time of the fluid. As a result, it is also interesting to study the ''supercooled'' regime, which would correspond to an equilibrated situation in the absence of a shear flow. Moreover, this way of probing the nonequilibrium properties of glassy systems is possibly more relevant experimentally than the aging approach, at least in the case of soft glassy materials.

Recently, a general scenario was proposed for glassy systems subject to an external forcing,[13] based on the study of simple ''mean-field'' models. The rationale of this approach is that the equilibrium dynamics of these models is equivalent to the ''schematic'' mode-coupling approach of slowing down in supercooled liquids.[14–16] The study of their nonequilibrium dynamics can thus be seen as a *nonequilib-*

 © 2002 American Institute of Physics

Downloaded 25 Jun 2007 to 128.135.152.55. Redistribution subject to AIP license or copyright, see http://jcp.aip.org/jcp/copyright.jsp

rium schematic mode-coupling approach.[17] In this respect, it is interesting to note that the mode-coupling theory was recently extended to the aging regime[18] with results that were first predicted from the study of mean-field models.[19,20] To our knowledge, the mode-coupling theory of supercooled fluid has not yet been extended to fluids under shear beyond the linear response of the supercooled regime, i.e., at equilibrium. However, in analogy to what was done for aging or supercooled systems, it seems sensible to bypass this aspect and to carry out a direct comparison between the predictions from mean-field theories and experimental or simulation results, with the hope that the general scenario is robust enough that the details of the system under study are relatively unimportant.

Several earlier studies have been devoted to simulating fluid under shear. Yamamoto and Onuki[21] concentrated their work on the understanding of the dynamics at the molecular level. Our study is focused on more global aspects, with the aim of providing some experimentally testable predictions. Liu and Nagel[22] also proposed to use the shear rate as a relevant control parameter for jamming systems. Liu and co-workers[23] investigated some aspects of the nonequilibrium dynamics of a model similar to ours, with the difference of being athermal (zero temperature) in the absence of shear. Some of their results are closely related to ours, as will be discussed in Secs. IV and VI. More phenomenological approaches may be found in Refs. 2, 10, and 24.

The aim of the present work is to check, on a realistic model of the fluid, some of the predictions that emerged from the earlier study of driven glassy systems.[13] For completeness, the main results of this study will be briefly recalled in Sec. II. In Sec. III, we describe our microscopic model for the fluid under shear. Sections IV and V describe our results for the dynamic properties of the fluid, both at the macroscopic (rheological) and at the microscopic (wave-vector-dependent correlations) scales. Sections VI and VII are devoted to one of the most important predictions of the mean-field scenario, namely the manner in which the equilibrium fluctuation–dissipation theorem is violated in such nonequilibrium systems and the resulting notion of an effective temperature. Section VIII proposes a numerical realization of a very simple experimental protocol to measure the effective temperature through a nonequilibrium generalization of the equipartition theorem. We discuss experimental and theoretical consequences of our results in Sec. IX.

II. SUMMARY OF THE NONEQUILIBRIUM MODE-COUPLING RESULTS

To make the paper self-contained, we briefly recall in this section the main results and predictions obtained within the mean-field approach of Ref. 13. In this paper, a simple system, the *p*-spin mean-field model, was studied under conditions that involved a constant energy input from an external driving force, analogous to the effect of a shear flow on a fluid. The resulting stationary nonequilibrium state was studied as a function of the temperature T and external drive, the intensity of which will be, for convenience, denoted by σ.

For $\sigma=0$, the model has an ideal glass transition at a finite temperature T_c where the relaxation time diverges. For $T>T_c$, the correlation functions are described by usual mode-coupling integrodifferential equations[15] and display the characteristic two-step relaxation predicted by these equations, the α and β relaxations. Below T_c, the system cannot equilibrate and displays aging behavior.[20]

Under a finite external drive, $\sigma\neq 0$, the system is stationary at all temperatures. For $T\lesssim T_c$, and in the asymptotic limit $\sigma\to 0$, the correlation functions retain the characteristic two-step shape of the equilibrium system, with an α-relaxation time that depends on σ. For $T<T_c$, this relaxation time diverges as $\sigma\to 0$, while for $T>T_c$ it goes to its equilibrium value in this limit. Although the driving force strongly influences the α relaxation, it does so by keeping the shape of the decay of the correlation unchanged. This leads to the property that correlation functions may be collapsed by a simple rescaling of the time. This scaling property is analogous to the time–temperature superposition property found at equilibrium, and we shall denote this prediction by ''time-shear superposition property.''

Based on a power dissipation argument, we were able for this simple system to define quantities equivalent to the viscosity and shear rate in a fluid under shear. This viscosity was found to have a characteristic shear-thinning behavior, decreasing for increasing shear rates as a power law. The shear-thinning exponent is equal to 2/3 for $T>T_c$, while for $T<T_c$, the viscosity diverges as $\sigma\to 0$, and the shear-thinning exponent appears to depend on temperature with a value between 2/3 and 1.

The behavior of the effective temperature was also investigated as a function of T and σ. We recall here that the effective temperature $T_{\rm eff}$ is *defined*, in a system invariant under time translation, by the relationship[19]

$$R(t)=-\frac{1}{k_B T_{\rm eff}(C)}\frac{dC(t)}{dt}. \tag{1}$$

Here $R(t)$ and $C(t)$ are, respectively, a response function and the associated correlation function. In equilibrium, the fluctuation–dissipation theorem can be written as $T_{\rm eff}(C)=T$. In the sheared system, the effective temperature was found, for $T<T_c$, to be a discontinuous function of C in the limit $\sigma\to 0$. For $C>q$, one has $T_{\rm eff}=T$, while for $C<q$, one finds $T_{\rm eff}(C)=T_{\rm eff}>T$, denoting an effective temperature larger than the bath temperature for long time scales.[19] The parameter q is the plateau value of the correlation function: it is called the Edwards–Anderson parameter in the literature of disordered systems, or the nonergodicity parameter in the language of mode-coupling theory. At finite shear, the effective temperature also has an almost discontinuous behavior as a function of C. For $T>T_c$, the discontinuity decreases and vanishes when $\sigma\to 0$, so that equilibrium behavior is recovered in this limit.

An important outcome of theoretical studies of the concept of effective temperature for the slow modes of a glassy system is that the value of the effective temperature is independent, at the mean-field level, of which observable is chosen to compute correlation and response functions.[18,19,25,26] This prediction was recently challenged within a simple trap model,[27] with negative results. We will see in Sec. VI that

Downloaded 25 Jun 2007 to 128.135.152.55. Redistribution subject to AIP license or copyright, see http://jcp.aip.org/jcp/copyright.jsp

this important prediction is nicely verified in our realistic model.

The simple mean-field model studied in Ref. 13 does not allow any discussion of spatial dependency. However, characteristic features of the spatial dependence usually expected from the solution of mode-coupling-like equations will be investigated in Sec. V C.

III. MODEL AND DETAILS OF THE SIMULATION

The system simulated in this work is a 80:20 mixture of $N=2916$ Lennard-Jones particles of types A and B, with interaction

$$V(\mathbf{r}_{\alpha\beta})=4\varepsilon_{\alpha\beta}\left[\left(\frac{\sigma_{\alpha\beta}}{|r_{\alpha\beta}|}\right)^{12}-\left(\frac{\sigma_{\alpha\beta}}{|\mathbf{r}_{\alpha\beta}|}\right)^{6}\right], \tag{2}$$

where α and β refer to the two species A and B. Interaction parameters are chosen to prevent crystallization.[28] In all the paper, the length, energy, and time units are the standard Lennard-Jones units σ_{AA} (particle diameter), ε_{AA} (interaction energy), and $\tau_0=(m_A\sigma_{AA}^2/\varepsilon_{AA})^{1/2}$,[29] where m_A is the particle mass and the subscript A refers to the majority species. Particles have equal masses, and the interaction parameters are $\varepsilon_{AB}=1.5\varepsilon_{AA}$, $\varepsilon_{BB}=0.5\varepsilon_{AA}$, $\sigma_{BB}=0.88\sigma_{AA}$, $\sigma_{AB}=0.8\sigma_{AA}$. With these interaction parameters between species, equilibrium properties of the system have been fully characterized.[28] At the reduced density $\rho=1.2$, where all our simulations are carried out, a ''computer glass transition'' is found in the vicinity of $T_c\sim 0.435$. The slowing down of the dynamics, $T\gtrsim 0.45$, is correctly described by mode-coupling theory, which breaks down when lowering further the temperature, $T\lesssim 0.45$.[28] The aging behavior of the system below this temperature has also been characterized extensively, including the violation of the fluctuation–dissipation theory in the glassy phase.[30]

In order to study the system under a steady shear flow, the classical Newton equations are replaced by the so-called Sllod equations[31] (so named because of the relationship to the Doll's tensor algorithm)

$$\begin{aligned}\frac{d\mathbf{r}_i}{dt}&=\frac{\mathbf{p}_i}{m_i}+\mathbf{r}_i\cdot\boldsymbol{\nabla}\mathbf{v},\\ \frac{d\mathbf{p}_i}{dt}&=-\sum_{j\neq i}\frac{\partial V(\mathbf{r}_{ij})}{\partial\mathbf{r}_{ij}}-\mathbf{p}_i\cdot\boldsymbol{\nabla}\mathbf{v},\end{aligned} \tag{3}$$

where $(\mathbf{p}_i,\mathbf{r}_i)$ are the momentum and position of particle i, respectively. These equations are integrated by a standard leapfrog algorithm,[32] where time is discretized. The value $\Delta t=0.01$ was used throughout the simulations. Lees–Edwards boundary conditions[32] are used in a cubic simulation box of linear size $L=13.4442$. With these boundary conditions the flow is homogeneous, and no instability, such as shear-banding, was observed in our simulations.[33,34] Note also that this is the shear rate γ which is controlled in our simulations. The velocity gradient is in the y direction, and the fluid velocity in the x direction, i.e., $\mathbf{v}=\gamma y\mathbf{e}_x$. Constant temperature conditions are ensured by a simple velocity rescaling of the z component of the velocities, at each time step.[35]

The shear rate γ naturally introduces a new time scale γ^{-1} into the problem. Obviously, a simulation involving a steady shear state is possible only if the available simulation time is significantly larger than γ^{-1}. This limits our study to shear rates larger than typically $10^{-4}\tau_0$, corresponding to 10^6 time steps. The temperature range studied here is $T\in[0.15,0.6]$, which covers the liquid and glassy phases, while the shear rates $\gamma\in[10^{-4},0.1]$ which covers the linear and nonlinear response regimes of rheology. All the data presented in the following, even those below T_c, are obtained in a stationary state. This is unusual for systems below the glass transition temperature, which normally exhibit a nonstationary aging behavior.

IV. MACROSCOPIC BEHAVIOR: NONLINEAR RHEOLOGY

In this section, we study the rheological behavior of the system. Our results are very similar to that obtained in many different soft condensed-matter systems, making the Lennard-Jones mixture—which was originally designed as a model for simple metallic glasses—a reasonable one for more complex systems.

Before discussing our results, let us briefly recall some possible behaviors for the flow curves (stress σ as a function of shear rate) obtained in complex fluids. These results are often represented in the phenomenological form[1,2]

$$\sigma\approx\sigma_0+\alpha\gamma^n. \tag{4}$$

The case $n=1$ corresponds to Bingham fluids, with a yield stress σ_0, which vanishes for Newtonian systems. For $n<1$, Eq. (4) is often called the Hershel–Bulkeley law.[1] For zero yield stress ($\sigma_0=0$), Eq. (4) describes a power-law fluid, where the viscosity η decreases with increasing shear rate as a power law, $\eta\sim\gamma^{-\alpha}$, $\alpha\equiv 1-n$. Although these types of flow curves are found in many different complex systems, they are not usually supported by a theoretical basis and should therefore be interpreted as a convenient representation of the results on a limited range of shear rates. In our system, the microscopic stress σ_{xy} is defined by the usual formula

$$\sigma_{xy}\equiv\frac{1}{L^3}\left(\sum_{i=1}^{N}-\frac{p_{ix}p_{iy}}{m_i}+\sum_{i=1}^{N}\sum_{j>i}r_{ijx}\frac{\partial V(\mathbf{r}_{ij})}{\partial r_{ijy}}\right). \tag{5}$$

The shear-rate-dependent viscosity is defined by the ratio

$$\eta\equiv\frac{\sigma_{xy}}{\gamma}. \tag{6}$$

Figure 1 presents the flow curves $\sigma(\gamma,T)$ for various temperatures. The same data are also represented in the alternative form of viscosity versus shear rate. Two different regimes can be distinguished in these figures. For $T>T_c$, the behavior becomes Newtonian at low shear rates,

$$\sigma\approx\eta_0(T)\gamma, \tag{7}$$

where

$$\eta_0(T)=\lim_{\gamma\to 0}\eta(\gamma,T>T_c) \tag{8}$$

Downloaded 25 Jun 2007 to 128.135.152.55. Redistribution subject to AIP license or copyright, see http://jcp.aip.org/jcp/copyright.jsp

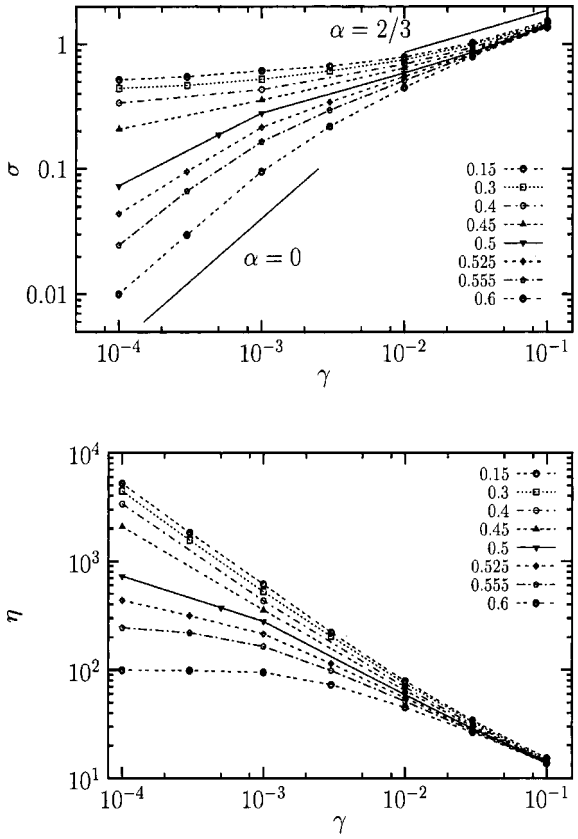

FIG. 1. Top: Flow curves $\sigma(\gamma)$ for various temperatures. Full lines are Newtonian behavior ($\alpha=0$) and shear-thinning behavior with $\alpha=2/3$. Bottom: Flow curves presented in the alternative form $\eta(\gamma)$, for the same temperatures.

is the viscosity of the fluid in the linear regime. We have checked that it is proportional to the equilibrium relaxation time of the fluid,[21] and it is found to diverge as the temperature is lowered as a power law $\eta_0(T)\sim(T-T_c)^{-2.45}$, in good agreement with equilibrium simulations.[28] Figure 2 shows that in this temperature regime, all the data can be rescaled onto a master curve of the form

$$\eta(\gamma,T)=\frac{\eta_0(T)}{[1+\gamma/\gamma_0(T)]^{2/3}}. \tag{9}$$

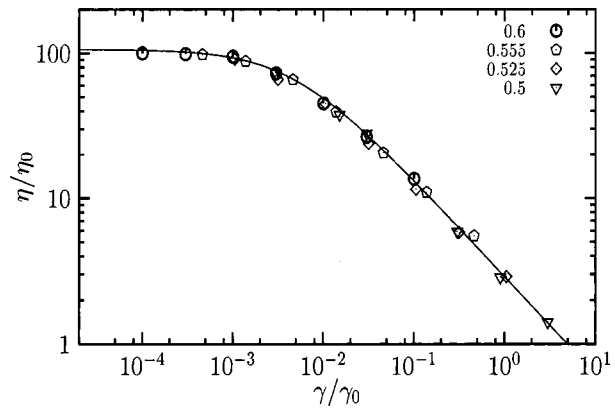

FIG. 2. Scaling behavior of the flow curves $\eta(\gamma)$ for various temperatures above T_c. The full line is a fit to Eq. (9).

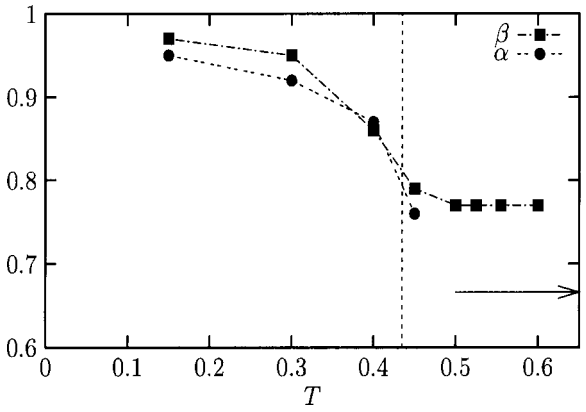

FIG. 3. Evolution of the effective shear-thinning exponent $\alpha(T)$ and of the stretching exponent $\beta(T)$. The horizontal arrow shows the value $\alpha=\frac{2}{3}$ obtained above T_c. The vertical dashed line is at $T_c=0.435$.

$\gamma_0(T)$ is not a free parameter, but has the form $\gamma_0(T)\sim(T-T_c)^{-2.45\times3/2}$, which ensures that the divergence of the viscosity at T_c is a power law $\eta(\gamma,T_c)\sim\gamma^{-2/3}$.

Equation (9) describes a crossover between a Newtonian behavior at small shear rates and a power law behavior with $\eta\sim\gamma^{-2/3}$ at higher shear rates. Remarkably, the same behavior, with the same exponent 2/3, was predicted by the mean-field theory of Ref. 13. This coincidence, however, is not necessarily significant. A similar shear-thinning behavior, $\eta\sim\gamma^{-\alpha}$, with exponents in the range $\alpha=0.5$–1.0 is obtained in many different soft systems, such as suspensions and concentrated polymer solutions.[1,36] Confined polymer layers under constant normal load[37] were also found to exhibit very similar shear-thinning behavior. In our case, the data could probably be fitted with a slightly different value for the exponent, and the choice of $\frac{2}{3}$ is motivated by theoretical results.[13]

At low temperatures, the curves shown in Fig. 1 present a crossover between two shear-thinning regimes. For relatively high shear rates, they can be described by the same shear-thinning exponent as above T_c, $\alpha=2/3$, but at low shear rates, the shear-thinning behavior is more marked, $\alpha>\frac{2}{3}$. One can define an effective shear-thinning exponent from the slope of the curves in Fig. 1 [$\alpha=d\ln\eta/d\ln\gamma$)]. It crosses over from $\alpha\sim\frac{2}{3}$ at a relatively high shear rate to a larger value for the lowest shear rate investigated here. The temperature dependence of the latter is reported in Fig. 3, which shows that $\alpha(T)$ saturates to 1 when $T\to0$, which seems to indicate that the system has a finite yield stress in this limit only.

Although our results are obtained over three decades of shear rates, we cannot report a definite functional form for the flow curves. An alternative view of the low-temperature flow curves is that the effective shear-thinning exponent will saturate to the value $\alpha(T)=1$ in the (numerically unreachable) very low shear rate limit, indicating the existence of a yield stress $\sigma_0(T)\equiv\lim_{\gamma\to0}\sigma(\gamma,T)$ for the system at finite temperatures. Hence, we also tried to use Eq. (4), in order to extract a possible value of $\sigma_0(T)$. Note that this is made possible by the fact that Eq. (4) has more free parameters than a single power law. Fits are thus satisfactory, and the

Downloaded 25 Jun 2007 to 128.135.152.55. Redistribution subject to AIP license or copyright, see http://jcp.aip.org/jcp/copyright.jsp

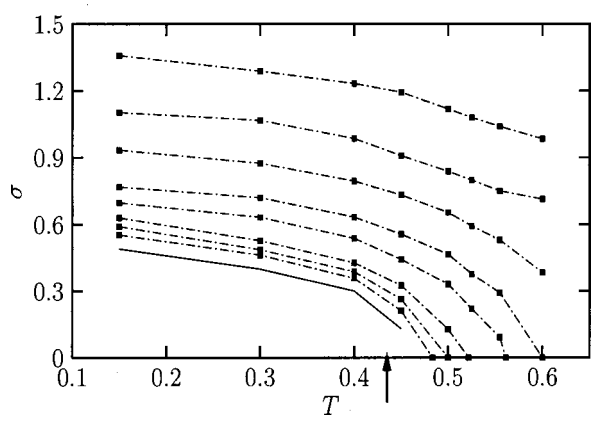

FIG. 4. The (σ,T) plane of the jamming phase diagram. The dashed curves are the viscosity contour plots. $\eta=20$, 30, 50, 100, 200, 500, 1000, and 2000 (from top to bottom). The full line represents the value of the yield stress $\sigma_0(T)$, extrapolated from Eq. (4). Arrow marks the mode-coupling temperature T_c.

values of the yield stress obtained at different temperatures in this manner are reported in Fig. 4. This ''jamming phase diagram'' is very similar to the one proposed by Liu and Nagel[22] and studied experimentally in Ref. 38. It is also an interesting way of thinking of the glass transition, and as such was theoretically investigated in Ref. 13. The ''jammed phase'' would correspond here to the low-σ, low-T part of the diagram.

V. MICROSCOPIC CORRELATION FUNCTIONS

The shear rate may be viewed as a new control parameter to access the glassy phase. As discussed earlier, one may expect scaling properties of the correlation functions as a function of shear rate to be similar to those observed when temperature is decreased. This basic remark was already made in Ref. 21, but we now have a clear theoretical context in which these results may be understood.[13] In this section, we briefly consider the influence of the shear rate on static correlations and investigate next the scaling properties of the time-dependent correlation functions.

A. Static correlation functions

Static correlations may be characterized through the structure factors of the fluid, defined as

$$S(\mathbf{k})=\frac{1}{N}\sum_{j=1}^{N}\sum_{l=1}^{N}\langle\exp\{i\mathbf{k}\cdot[\mathbf{r}_j(t_0)-\mathbf{r}_l(t_0)]\}\rangle. \tag{10}$$

We show first in Fig. 5 the structure factor for $\gamma=10^{-3}$ and $T=0.3$ in the three spatial directions. It can be seen that the flow, somehow surprisingly, introduces no obvious anisotropy in this structural quantity.[21] This can be explained by the fact that we are working at shear rates that are small, $\gamma\tau_0\ll 1$. A structural anisotropy would probably be present for larger shear rates, $\gamma\tau_0\gtrsim 1$.

We present next in Fig. 6 the evolution of $S(k_z)$ for different shear rates at constant temperature $T<T_c$. The ''glassy'' state is thus approached when the shear rate is lowered. We shall see below that for these values of the shear rate, the relaxation time increases by nearly two orders of magnitude. Only weak changes in the static structure factor are observed in the same shear rate window. The situation is thus strongly reminiscent of the observation made at equilibrium that no structural sign of the glass transition can be observed.[28,39]

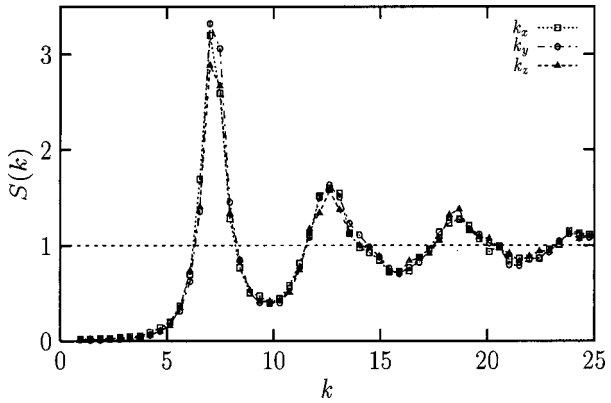

FIG. 5. Structure factor at fixed temperature, $T=0.3$, and shear rate, $\gamma=10^{-3}$, for the different orientations with respect to the flow.

B. α relaxation and ''time-shear superposition''

To investigate the dynamics of the fluid under shear, we focus on the number density fluctuations $\langle\delta\rho(\mathbf{k},t)\times\delta\rho(-\mathbf{k},t')\rangle$ where

$$\delta\rho(\mathbf{x},t)=\left\langle\frac{1}{N}\sum_{j=1}^{N}\delta(\mathbf{x}-\mathbf{r}_j(t))-\rho\right\rangle \tag{11}$$

is the density fluctuation at point $\mathbf{x}$ and time t, ρ being the average density of the fluid. For simplicity, we will limit ourselves to $\mathbf{k}$ vectors orthogonal to the flow directions, for which the overall motion of the fluid does not affect the correlation function directly.

To discuss the dynamic behavior of the system, we concentrate on the self-part of the intermediate scattering function, defined by

$$C_{\mathbf{k}}(t)=\frac{1}{N_A}\sum_{j=1}^{N_A}\langle\exp\{i\mathbf{k}\cdot[\mathbf{r}_j(t+t_0)-\mathbf{r}_j(t_0)]\}\rangle. \tag{12}$$

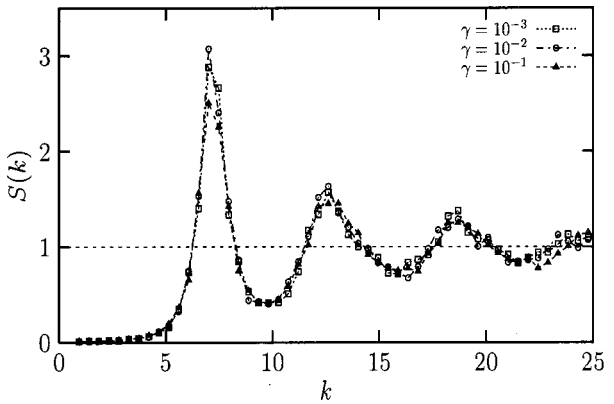

FIG. 6. Structure factor at fixed temperature $T=0.3$ and different shear rates. The relaxation time increases by ~ 2 orders of magnitude on the same shear rate interval.

Downloaded 25 Jun 2007 to 128.135.152.55. Redistribution subject to AIP license or copyright, see http://jcp.aip.org/jcp/copyright.jsp

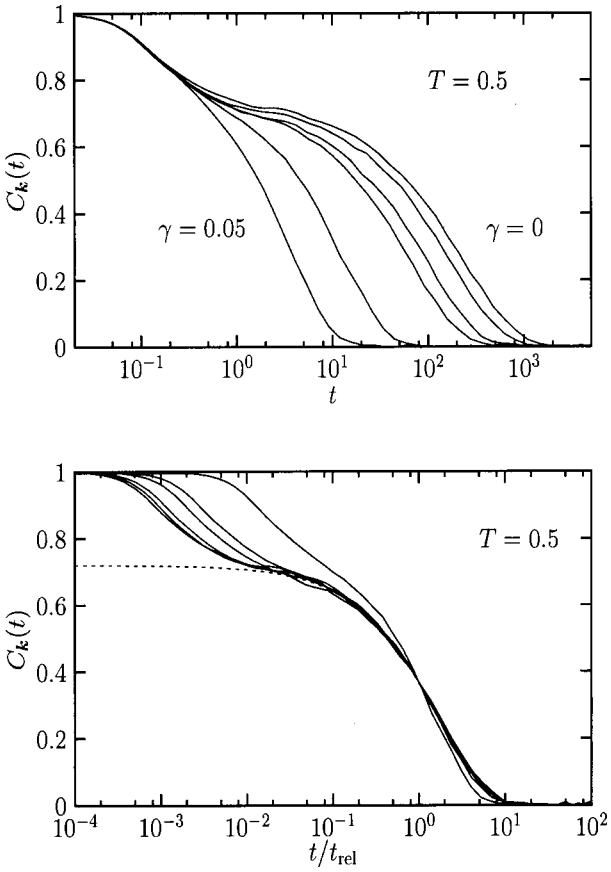

FIG. 7. Top: Correlation functions for $T=0.5>T_c$ and different values of the shear rate, $\gamma=0$, 10^{-4}, 5×10^{-4}, 10^{-3}, 10^{-2}, 5×10^{-2} (from right to left). Bottom: The slow decay of the correlation function can be collapsed if the time is rescaled by $t_{\rm rel}(\gamma)$. The dashed line is a fit to a stretched exponential form, with an exponent $\beta=0.77$.

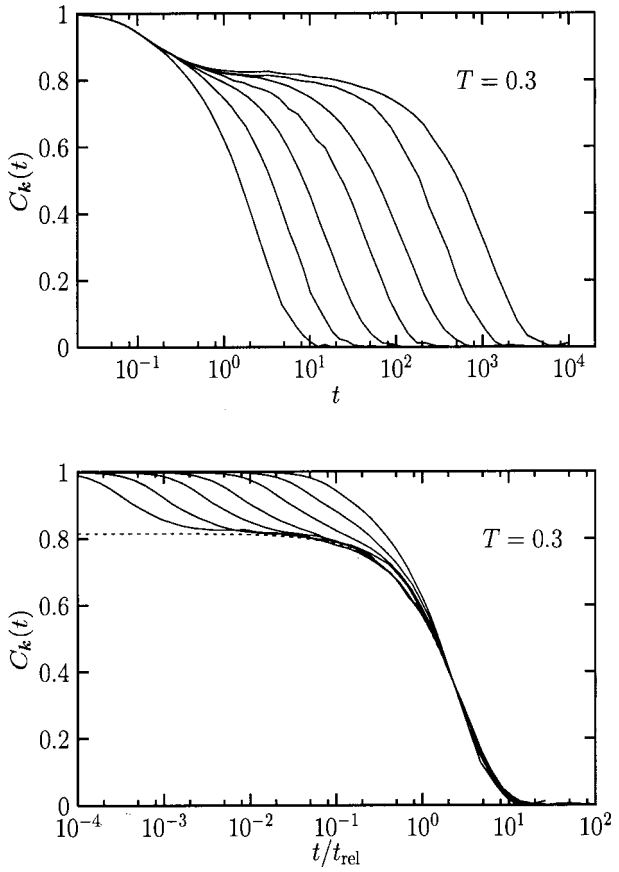

FIG. 8. Top: Correlation functions for $T=0.3<T_c$ and different values of the shear rate, $\gamma=10^{-4}$, 3×10^{-4}, 10^{-3}, 3×10^{-3}, 10^{-2}, 3×10^{-2}, 10^{-1} (from right to left). Bottom: The slow decay of the correlation function can be collapsed if the time is rescaled by $t_{\rm rel}(\gamma)$. The dashed line is a fit to a stretched exponential form, with an exponent $\beta=0.95$.

We have also computed this function for the minority species, *B*, with very similar results that will not be discussed here. These correlation functions are displayed for two different temperatures and several shear rates in Figs. 7 and 8. The wave vector is $\mathbf{k}=7.47\mathbf{e}_z$, which corresponds to the peak of the structure factor (see Fig. 5). The overall shape is very similar to what is usually found in supercooled systems, namely a first ''microscopic'' relaxation that is independent of the control parameters, followed by a slow approach to a ''plateau'' that we will describe as β relaxation in analogy with the mode-coupling terminology. The decay beyond the plateau, or terminal relaxation, will be described as α relaxation. Obviously, the α-relaxation time is a strongly decreasing function of shear rate.[40]

It is a theoretical prediction that the slow decay of the correlation function may be collapsed by a simple rescaling of the time, the time-shear superposition property.[13] As in equilibrium,[28] the relaxation time is defined from the relation $C_{\mathbf{k}}(t_{\rm rel})\equiv e^{-1}$. The scaling form

$$C_{\mathbf{k}}(t)=F_{\mathbf{k}}\left(\frac{t}{t_{\rm rel}(\gamma)}\right), \tag{13}$$

where the function $F_{\mathbf{k}}(x)$ is a master function that may depend on temperature, is tested in Figs. 7 and 8. It can be seen that such a scaling is indeed nicely obeyed for the α relaxation of the correlation functions. The scaling function is correctly described by a stretched exponential,

$$F_{\mathbf{k}}(x)\approx\exp(-x^{\beta(T)}), \tag{14}$$

with the stretching exponent $0<\beta(T)<1$. The temperature evolution of $\beta(T)$ is shown in Fig. 3, which demonstrates that the decay becomes less stretched when the temperature is lowered. The stretching exponent seems to saturate to the value 1 as *T* decreases to 0. In this figure, a close relationship between this stretching of the correlation function and the shear-thinning exponent is also clearly apparent. This is physically plausible: $\beta=1$ corresponds to a pure exponential form, i.e., a single relaxation time; $\beta<1$, on the other hand, is associated with a broader distribution of relaxation times. If $\beta=1=\alpha$, there is a single relevant time scale, and the scaling $\eta\sim\gamma^{-1}\sim t_{\rm rel}$ shows that this time scale is simply given by the inverse of the shear rate, as would be obtained by a naive dimensional analysis. This suggests, as an interesting corollary, that a shear-thinning exponent $\alpha<1$ implies the existence of a broad distribution of time scales.

C. Spatial dependence and β relaxation

The wave-vector dependence of the number–number correlation function is displayed in Fig. 9. As usual,[28] the

Downloaded 25 Jun 2007 to 128.135.152.55. Redistribution subject to AIP license or copyright, see http://jcp.aip.org/jcp/copyright.jsp

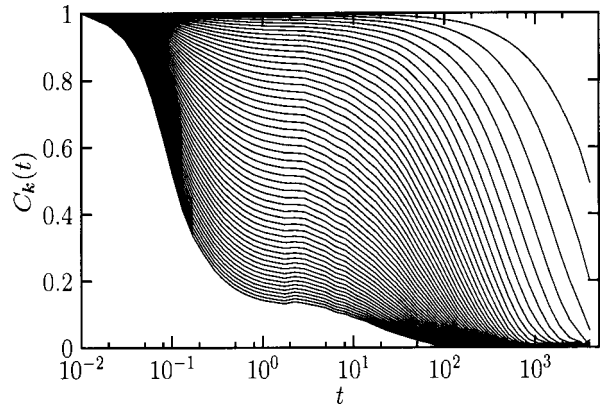

FIG. 9. Correlation function for $T=0.3$, $\gamma=10^{-3}$, and different values of the wave vector regularly spaced between $k=0.93$ and $k=24.76$ (from top to bottom).

overall shape is qualitatively the same for all wave vectors, the plateau value and the stretching exponent being simple functions of the wave vector.

In mode-coupling theories,[16,18] an interesting and easily testable property of the correlation function is the so-called ''factorization property,'' which characterizes the spatial dependence in the β-relaxation region. This factorization property can be written, for the correlation function under study, in the form $C_{\mathbf{k}}(t)=q_k+h_k f(t)$, where q_k is the wave-vector-dependent Edwards–Anderson parameter, and $f(t)$ a universal function, i.e., independent of the chosen correlation function. More generally, it implies that in the β regime the ratio

$$R_\varphi(t)=\frac{\varphi(t)-\varphi(t'')}{\varphi(t')-\varphi(t'')}, \tag{15}$$

where $\varphi(t)$ is any slow observable [e.g., $C_{\mathbf{k}}(t)$], and t, t' and t'' are in the β-relaxation window, is independent of the observable.[28,30]

This prediction is tested in Fig. 10, which shows that the ratios (15) obtained for different wave vectors are indeed independent of the wave vector. Again, these data are very similar to what is observed at equilibrium[28] and in the aging regime.[30]

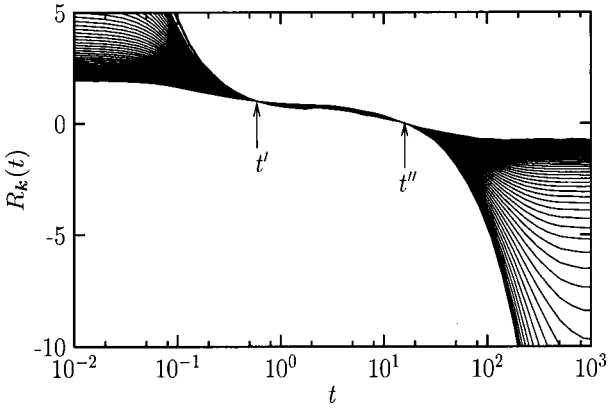

FIG. 10. The correlation functions of Fig. 9 are rescaled in the β regime using the mode coupling called ''factorization property'' [Eq. (15)]. Times are $t'=0.57$ and $t''=14$, as indicated by the arrows.

VI. EFFECTIVE TEMPERATURES

A. Existence of an effective temperature

Nonequilibrium mean-field or mode-coupling theories have shown that whereas correlation functions were the only relevant quantities to be studied at equilibrium, it is of primary interest to separatly study susceptibilities in out of equilibrium situations.[13,18–20] At equilibrium, these two families of dynamic functions are related by fluctuation–dissipation theorems (FDT's). In nonequilibrium situations, FDT is *a priori* not satisfied. However, it now is clear that the study of the corrections to the FDT are relevant.[4] Recent theories of nonequilibrium systems have indeed introduced the notion of effective temperature associated with the modification of the fluctuation–dissipation theorem.[19,26] This effective temperature is defined by the ratio of the response to correlation function in the following way. Consider two physical observables $O(t)$ and $O'(t)$. The correlation function $C_{OO'}(t)$ is defined as

$$C_{OO'}(t)=\langle O(t+t_0)O'(t_0)\rangle-\langle O(t_0)\rangle\langle O'(t_0)\rangle, \tag{16}$$

where t_0 is an arbitrary initial time and $\langle\cdots\rangle$ indicates an average over different initial times t_0. The conjugated response function is defined by

$$R_{OO'}(t)=\frac{\delta\langle O(t+t_0)\rangle}{\delta h_{O'}(t_0)}, \tag{17}$$

where $h_{O'}$ is the field thermodynamically conjugated to $O'(t)$. In a system at thermodynamic equilibrium, the FDT reads

$$R_{OO'}(t)=-\frac{1}{T}\frac{dC_{OO'}(t)}{dt}. \tag{18}$$

The more easily accessible physical quantity is the susceptibility

$$\chi_{OO'}(t)=\int_0^t dt' R_{OO'}(t'), \tag{19}$$

which is obtained by applying a small, constant field $h_{O'}$ in the time interval $[0,t]$. In the linear response regime, $h_{O'}\to 0$, one gets

$$\chi_{OO'}(t)\approx\frac{\langle O(t)-O(0)\rangle}{h_{O'}}. \tag{20}$$

The equilibrium FDT thus implies a linear relation between the susceptibility and the correlation, namely,

$$\chi_{OO'}(t)=\frac{1}{T}[C_{OO'}(0)-C_{OO'}(t)]. \tag{21}$$

In a system out of equilibrium, the FDT is not expected to hold. However, in a system invariant under time translation, a modified version of Eq. (18) can be used to *define* the functions $T_{\rm eff}^{OO'}(C_{OO'})$ through[19]

$$R_{OO'}(t)=-\frac{1}{T_{\rm eff}^{OO'}(C_{OO'})}\frac{dC_{OO'}(t)}{dt}. \tag{22}$$

The $T_{\rm eff}^{OO'}(x)$ are *a priori* arbitrary functions of their argument, and may depend on which observables $O(t)$ and $O'(t)$

Downloaded 25 Jun 2007 to 128.135.152.55. Redistribution subject to AIP license or copyright, see http://jcp.aip.org/jcp/copyright.jsp

are under study. However, *they can be measured* by following the same linear response procedure as in the equilibrium case, so that

$$\chi_{OO'}(t)=\int_0^t dt'\left(-\frac{1}{T_{\rm eff}^{OO'}(C_{OO'})}\frac{dC_{OO'}(t')}{dt'}\right)$$
$$=\int_{C_{OO'}(t)}^{C_{OO'}(0)}\frac{dx}{T_{\rm eff}^{OO'}(x)}. \tag{23}$$

The existence of an effective temperature is thus *demonstrated* if a straight line is obtained in a susceptibility–correlation plot parametrized by the time. As was shown in several cases,[26] the same system may exhibit different temperatures on different time scales. If this is the case, the parametric plot will consist in several different straight lines, the slope of each line determining an effective temperature. Cases are also known[41,42] in which the parametric plot is ill-defined at short times (e.g., because of an oscillatory behavior of the correlation function) but yields a well-defined effective temperature on longer time scales. It is therefore generally *incorrect* to define an effective temperature through the approximate expression $\chi_{OO'}(t\to\infty)/C_{OO'}(0)$, as is sometimes done.[23] This corresponds to taking the average slope of the parametric plot as an effective temperature, therefore losing all information on the time scale dependence of the effective temperature.

Obviously, the introduction of an effective temperature is of ''thermodynamic'' interest only if this quantity is actually independent of the observables $O(t)$ and $O(t')$ under consideration, $T_{\rm eff}^{OO'}\equiv T_{\rm eff}$. This is true at the mean-field level,[18,19,25] and this question will be investigated in detail below.

As a first investigation of the existence and behavior of the effective temperature and fluctuation–dissipation relation, we consider the case of single-particle density fluctuations, for which the corresponding correlation function has been studied in detail above. Corresponding observables are in this case

$$O(t)=\frac{1}{N_A}\sum_{j=1}^{N_A}\varepsilon_j\exp[i\mathbf{k}\cdot\mathbf{r}_j(t)] \tag{24}$$

and

$$O'(t)=2\sum_{j=1}^{N_A}\varepsilon_j\cos[\mathbf{k}\cdot\mathbf{r}_j(t)], \tag{25}$$

where $\varepsilon_j=\pm1$ is a bimodal random variable of mean 0. The relation

$$C_{\mathbf{k}}(t)=\overline{C_{OO'}(t)}, \tag{26}$$

where the horizontal line means an average over the realizations of $\{\varepsilon_j\}$, easily follows. To compute the susceptibility, a force

$$\mathbf{F}_j(\mathbf{k},t)=-\frac{\partial}{\partial\mathbf{r}_j}[-h_{O'}O'(t)] \tag{27}$$

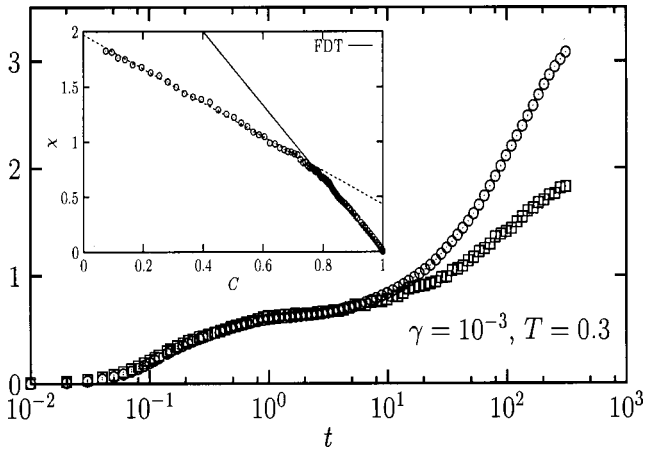

FIG. 11. Susceptibility $\chi_{\mathbf{k}}(t)$ (squares) and $[1-C_{\mathbf{k}}](t)]/T$ (circles) vs time, for $\mathbf{k}=7.47\mathbf{e}_z$, $T=0.3$, and $\gamma=10^{-3}$. The two curves are superposed when the equilibrium FDT is satisfied. Inset: Parametric susceptibility vs correlation plot for the same data. The dashed line is a linear fit to the small-C part of the data, with $T_{\rm eff}=0.65$. The full line is the equilibrium FDT.

is exerted on each A particle. The response function $\chi_{\mathbf{k}}(t)$ [see Eq. (20)] is computed by averaging the response obtained in different realizations of the $\{\varepsilon_j\}$.

The time dependence of the dynamic functions $\chi_{\mathbf{k}}(t)$ and $[1-C_{\mathbf{k}}(t)]/T$ is displayed in Fig. 11. In that case, 200 realizations of the $\{\varepsilon_j\}$ have been considered. This figure shows that the equilibrium FDT is obeyed at short times, and violated at larger times. From these functions, a parametric plot is built, as shown in the inset of Fig. 11. It can be seen that the parametric plot can be described to an excellent approximation by two straight lines, of slopes $-1/T$ (large value of the correlation corresponding to short times) and $-1/T_{\rm eff}$ (small value of the correlation corresponding to large times). This observation is thus in perfect agreement with the behavior predicted theoretically[13] and was the main result in Ref. 43.

B. Effective temperature in the plane (γ, T)

The effective temperature is defined as (minus) the inverse slope of the parametric susceptibility–correlation plot for long times. This effective temperature will, generally speaking, depend on how strongly the system is externally driven. One may ''reasonably'' expect that a stronger drive implies a higher effective temperature. (See the discussion of the word *reasonably* at the end of the paper.) That this is indeed the case is demonstrated in Fig. 12, where parametric susceptibility–correlation plots are displayed for several different shear rates.

Two different situations are considered in this figure. At high temperatures, $T>T_c$, the effective temperature reduces to the bath temperature when the shear rate is decreased. As predicted theoretically,[13] we find here that the effective temperature of the slow modes is equal to the bath temperature as long as the system is in its Newtonian regime, $\eta\sim$ const. This is physically reasonable, since the linear regime of rheology corresponds roughly to shear rates such that $\gamma t_{\rm rel}<1$, for which the dynamics is weakly affected.[13,21]

Downloaded 25 Jun 2007 to 128.135.152.55. Redistribution subject to AIP license or copyright, see http://jcp.aip.org/jcp/copyright.jsp

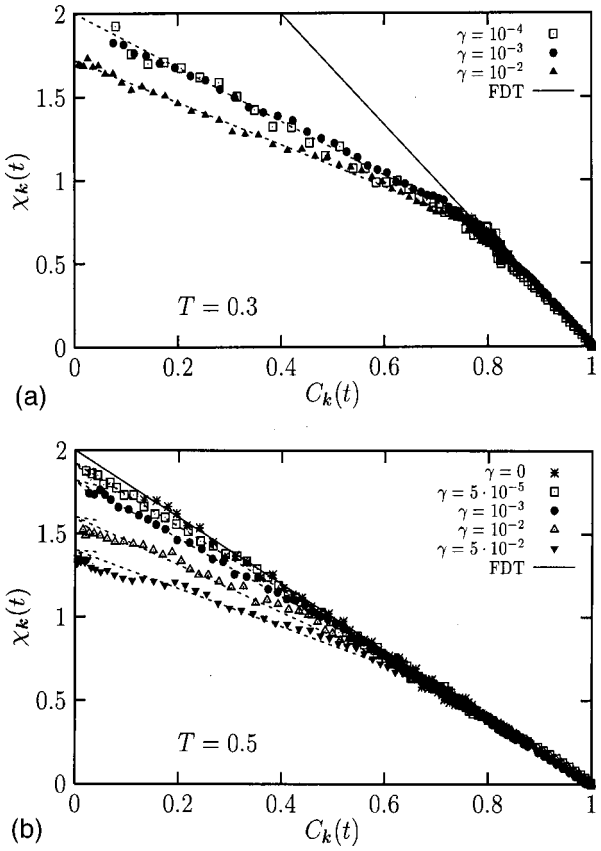

FIG. 12. Parametric plots for $T=0.3$ (top) and $T=0.5$ (bottom), and various shear rates. In both figures, the full line is the FDT, and has a slope $-1/T$. The dashed lines are linear fits to the small-C part of the data, for $\gamma>0$. The wave vector is $\mathbf{k}=7.47\mathbf{e}_z$ for all the curves of this figure.

In the ''glassy'' low-temperature region, on the other hand, the effective temperature also decreases with decreasing shear rate, but saturates for the lower shear rates that can be investigated in the simulation at a value different from the bath temperature, as theoretically predicted.[13] The existence of such a limiting value is physically interpreted by the fact that at low temperature, a Newtonian ($\eta\sim$const) or near-equilibrium ($T_{\rm eff}\sim T$) regime defined as above by the condition $\gamma t_{\rm rel}<1$ does not exist, since $t_{\rm rel}\sim\infty$.

The limiting value $T_{\rm eff}(\gamma\to 0)$ corresponds to the effective temperature that was observed in the corresponding *aging* studies of the same system at this temperature.[30] In Ref. 30, the limiting value $T_{\rm eff}\sim 0.62$ is reported (however, with much less accuracy than in the present paper), while we find $T_{\rm eff}\sim 0.65$ at the same temperature $T=0.3$. This is again expected from the theory,[13] and confirms the interpretation of $T_{\rm eff}$ as a signature of the geometry of phase space explored by the system on the simulation time scale, independently of the exact procedure that is followed.[13,19,42]

VII. OBSERVABLE INDEPENDENCE OF $T_{\rm eff}$

As we already mentioned, the notion of an effective temperature derived from the fluctuation–dissipation relation is much more relevant if it can be shown to not depend on the observable under consideration. That $T_{\rm eff}$ is observable independent is indeed one of the crucial predictions of mean-field approaches.[18,19,25] In this section, we explore this important issue by computing the susceptibility–correlation parametric plots for several different observables. Since the computation of response functions is numerically very demanding, the method we used consisted in computing very accurately the effective temperature from the scattering function for $\mathbf{k}=7.47\mathbf{e}_z$. From the data in Fig. 11, one has the estimation $T_{\rm eff}\simeq 0.65$ for $T=0.3$ and $\gamma=10^{-3}$. We can then compute for the same parameters (T,γ) the response associated with other observables, and check whether these data are compatible with this value of $T_{\rm eff}$. Since we have explained in some detail the generic numerical procedure to measure $T_{\rm eff}$ in the previous section, less details will be given here. Instead, we carefully discuss the possible experimental realizations of our measurements. Note that in experiments, a simultaneous measurement of the response and of the correlation is very difficult, and has been achieved only in very few cases.[44–47] While usual dielectric, magnetic, or mechanical methods yield response functions, scattering experiments probe only correlation functions.[5,9]

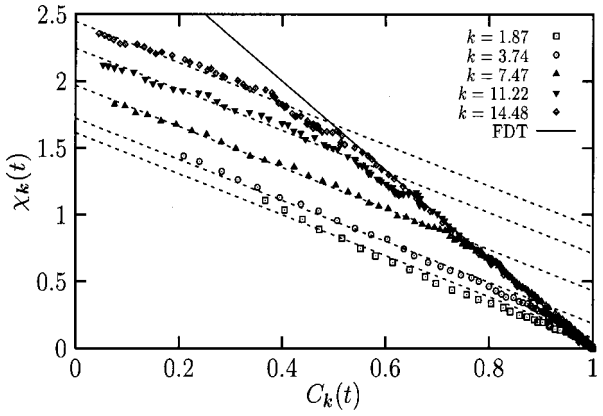

FIG. 13. Comparison of the parametric plot for $T=0.3$ and $\gamma=10^{-3}$, and different wave vectors in the direction z. The full line is the equilibrium FDT of slope $-1/0.3$, the dashed lines have slope $-1/0.65$.

A. Position correlations for different wave vectors

As a first check, we have investigated the wave-vector dependence of the parametric plot for the self-part of the intermediate scattering function. The results, displayed in Fig. 13, are indeed perfectly consistent with a wave-vector-independent effective temperature. Parametric plots for different wave vectors differ only through the value of the correlation function at which the crossover from bath to effective temperature takes place. This value marks the crossover between ''short,'' equilibrated and ''long,'' out-of-equilibrium time scales. It also corresponds to the plateau value q_k in the correlation functions displayed in Fig. 7. Note that the wave vectors studied here cover a range of length scales roughly between $0.5\sigma_{AA}$ and $4\sigma_{AA}$. That these different length scales have the same off-equilibrium behavior, as observed through the effective temperature, is not *a priori* obvious. It is in opposition, for instance, to the simple view of the system rapidly equilibrating its small length scales,

Downloaded 25 Jun 2007 to 128.135.152.55. Redistribution subject to AIP license or copyright, see http://jcp.aip.org/jcp/copyright.jsp

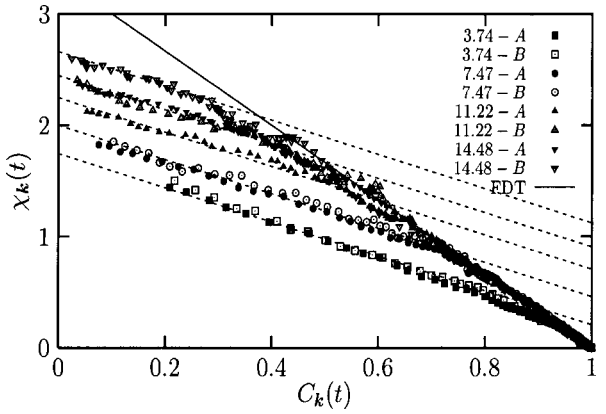

FIG. 14. Comparison of the parametric plot for $T=0.3$ and $\gamma=10^{-3}$, for the two types (A and B) of Lennard-Jones particles. The data are compatible with the same T_{eff} although the statistics for B particles, the minority species, is slightly not as good as for A particles. The full line is the equilibrium FDT of slope $-1/0.3$; the dashed lines have slope $-1/0.65$.

while its large length scales need much more time to reach equilibrium, a generic scheme which is put forward in systems such as spin glasses.[48]

The ''chemical'' dependence of the effective temperature can also be investigated by computing the correlation function $C_{\mathbf{k}}(t)$ and the corresponding response, associated with A and B particles of the Lennard-Jones binary mixture. The results, displayed in Fig. 14, again confirm that the slope of the parametric plots does not depend on the particular chosen observable, all the plots being well compatible with the same $T_{\text{eff}}=0.65$.

Finally, the collective correlation and response functions can also be computed—albeit with a bit less accuracy than the incoherent ones. This correspond to observables Eq. (24) and (25) but taking $\varepsilon_j \equiv 1$ for all j. The resulting parametric plots are shown in Fig. 15, for two different wave vectors. Again, slopes are perfectly compatible with equilibrium FDT for short times, and with $T_{\text{eff}}=0.65$ for longer times.

It is interesting to consider how such response–correlation plots could be obtained experimentally in soft condensed-matter systems. While the correlation functions are reasonably easily obtainable through light scattering

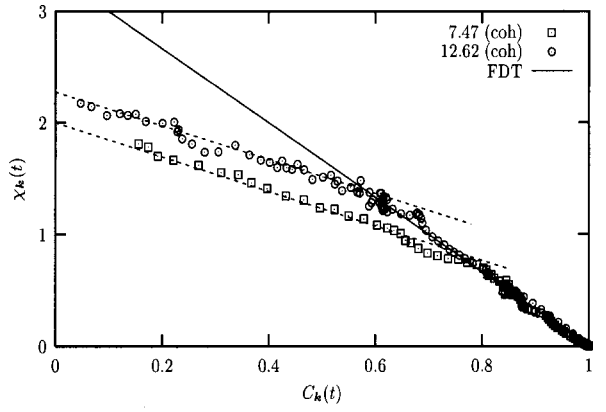

FIG. 15. Parametric plots from the coherent density fluctuations for two wave vectors $\mathbf{k}=7.47\mathbf{e}_z$ and $\mathbf{k}=12.62\mathbf{e}_z$. The full line is the equilibrium FDT of slope $-1/0.3$; the dashed lines have slope $-1/0.65$.

experiments,[5,9,49] the same is not true of response functions. In order to obtain the latter, one has to be able to manipulate the particles through some externally applied potential, modulated at the same wave vector as used in the light scattering experiment. One suggestion here would be to use some non-index-matched tracer particles in an index-matched colloidal suspension. The tracer particles would then be sensitive to the intensity of the local electric field. The same effect is used, e.g., in optical tweezers. An interference pattern would actually realize the modulated external potential considered in this section. Reading of the response could then be obtained from the scattering at the wavelength corresponding to this pattern.

B. Einstein relation for the Lennard-Jones particles

A quantity which is not directly related to the incoherent correlation function is the mean square displacement of a tagged particle. The response function that is associated with this quantity is the displacement induced by applying a small, constant external force to this tagged particle. Both quantities are linked by a fluctuation–dissipation theorem, called the Einstein relation in that context. To increase the statistics, we compute the mean square displacement of all particles of the same type, for example for the particle A; we measure

$$\Delta(t)=\frac{1}{2N_A}\sum_{j=1}^{N_A}\langle[z_j(t+t_0)-z_j(t_0)]^2\rangle. \tag{28}$$

Again, we focus on the direction transverse to the flow, for computational simplicity. The conjugated response function is then

$$\chi_0(t)=\frac{1}{N_A F_0}\sum_{j=1}^{N_A} F_j z_j(t+t_0), \tag{29}$$

where $z_j(t)$ is the transverse position of particle j at time t. The force $F_j=\varepsilon_j F_0$ is applied in the direction z between times t_0 and $t+t_0$. The FDT then reads $\chi_0(t)=\Delta(t)/T$.

At short times, the mean square displacement is ballistic, $\Delta(t)\sim t^2$. This ballistic regime is, as usual, followed by a diffusive regime $\Delta(t)\sim t$. A more extensive discussion of this quantity in the shear flow may be found in Ref. 21. The time behavior is similar for the induced displacement, as shown in Fig. 16. Hence, by construction, a linear relation is obtained in the diffusive regime in the parametric plot of χ_0 versus Δ. We confirm in Fig. 17 that, again, the effective temperature defined in this way is compatible with the value $T_{\text{eff}}=0.65$ already obtained above. This is true for the two types of the Lennard-Jones mixture (see Fig. 17).

One may therefore define T_{eff} by simply using the relation

$$T_{\text{eff}}=D\zeta \tag{30}$$

between the diffusion constant D and the friction coefficient ζ, which are defined, as usual, as

$$\Delta(t)\sim Dt, \quad \chi_0(t)\sim\frac{1}{\zeta}t, \tag{31}$$

Downloaded 25 Jun 2007 to 128.135.152.55. Redistribution subject to AIP license or copyright, see http://jcp.aip.org/jcp/copyright.jsp

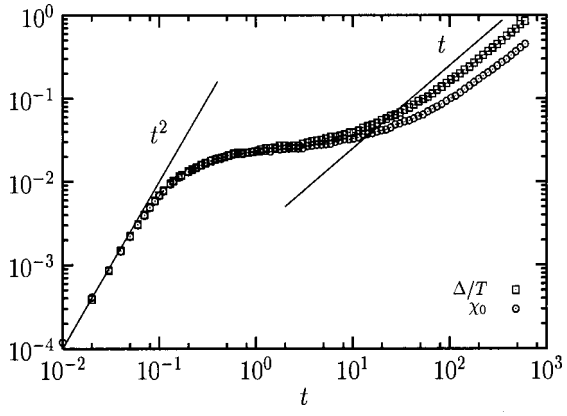

FIG. 16. Mean square displacement [Eq. (28)] normalized by the temperature, and induced displacement [Eq. (29)] as functions of time. At equilibrium, the FDT implies the equality of both quantities. Full lines are the power law behavior of ballistic (t^2) and diffusive (t) regimes.

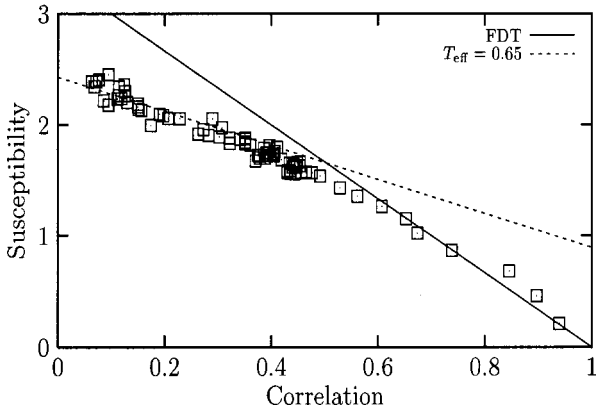

FIG. 18. Parametric plot for $T=0.3$ and $\gamma=10^{-3}$, for the stress fluctuations. The full line is the equilibrium FDT of slope $-1/0.3$; the dashed line has slope $-1/0.65$.

for times that are in the diffusive regime. This method was already used in Refs. 50–52 to extract an effective temperature in aging systems and in Ref. 53 in the context of sheared granular materials.

Its interest, especially in view of experimental realizations of these measurements, lies in the fact that the full time dependence of the correlation and response functions is not needed to extract the effective temperature. Again, experiments could be considered if tracer particles sensitive to an external force field (e.g., magnetic particles) could be introduced into the system, and their mobility ζ measured together with their diffusion constant D.

C. Stress fluctuations

A completely different observable, of relevance to all flow situations, is the stress defined in Eq. (5). In this section, we study thus the case in which the two observables $O(t)$ and $O'(t)$ are equal to the diagonal stress in the direction perpendicular to the velocity and velocity gradient, $O(t)=O'(t)=\sigma_{zz}(t)$. To add a field conjugated to the normal stress, a compression δL_z of the simulation box is realized by rescaling all particle coordinates at time $t=0$. In the limit of small compression, $\delta L_z/L_z \ll 1$, the Hamiltonian H of the system becomes indeed

$$H(\delta L_z)=H(\delta L_z=0)+\frac{\delta L_z}{L_z}V\sigma_{zz}+O\left(\left(\frac{\delta L_z}{L_z}\right)^2\right), \qquad (32)$$

where $V=L_xL_yL_z$ is the volume of the system. This proves that $\delta L_z L_x L_y$ is the field thermodynamically conjugated to σ_{zz} and allows us to access another check of the observable independence of $T_{\rm eff}$.

The resulting parametric plot is shown in Fig. 18. Although the data are more noisy than in the density correlation case, the FDT violations are very similar, and the value of $T_{\rm eff}$ is well compatible with all the others.

Again, it may be possible to carry out the experiment corresponding to this simulation. Experimentally, the off-diagonal component of the stress (rather than a diagonal one) would be used as the observable. In fact, preliminary results in this direction, using an extremely sensitive rheometer, have been obtained on aging colloidal systems by Bellon and Ciliberto.[45,46] The superposition of a continuous flow in order to obtain the fluctuations in a sheared system, however, would represent a difficult experimental challenge.

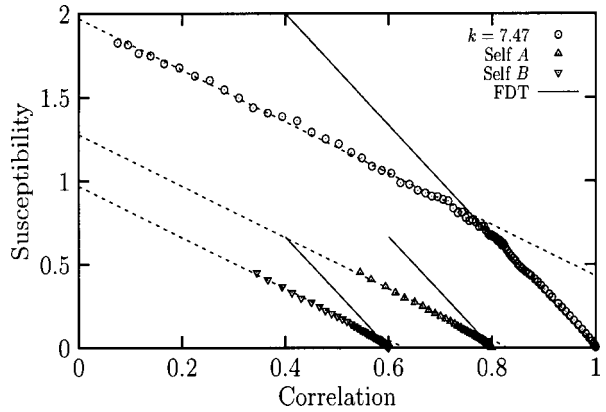

FIG. 17. Parametric plot for $T=0.3$ and $\gamma=10^{-3}$, for the self-diffusion of the two types of Lennard-Jones particles. We have represented the quantity χ_0 vs $x-\Delta$, where $x=0.6$ for B particles, $x=0.8$ for A particles, for graphical convenience. These curves are compared to the data obtained for the self part of the intermediate scattering function at $\mathbf{k}=7.47\mathbf{e}_z$. The full lines are the equilibrium FDT of slope $-1/0.3$; the dashed lines have slope $-1/0.65$.

VIII. FURTHER EXPERIMENTAL PROPOSALS: EQUIPARTITION THEOREM FOR THE SLOW MODES

As mentioned above, tracer particles can be used to probe the dynamics of the fluid. In particular, the Einstein relation between mobility and diffusion leads easily to the definition of an effective temperature, which appears to be identical to the one obtained from various susceptibility–correlation functions.

A different use of tracer particles is considered in this section, in which we investigate the dynamics of tracer particles with a mass large compared to that of the fluid particles. The idea is the following. The definition of $T_{\rm eff}$ as a ratio between correlation and response function has been shown to imply that if the fluid is used as a thermal bath to equilibrate a subsystem (or ''thermometer'') of typical time

Downloaded 25 Jun 2007 to 128.135.152.55. Redistribution subject to AIP license or copyright, see http://jcp.aip.org/jcp/copyright.jsp

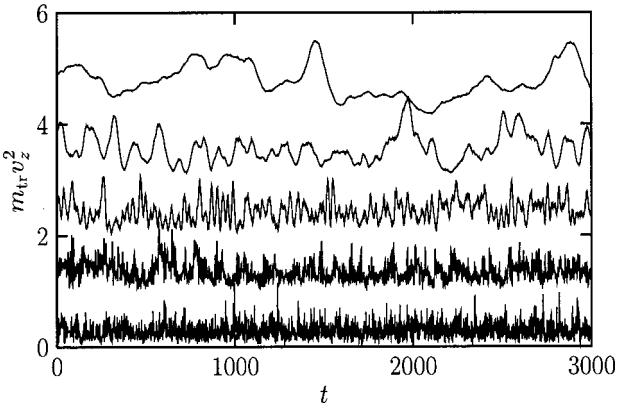

FIG. 19. Time dependence of the quantity $m_{tr}v_z^2$ in particular trajectories of tracer particle of mass $m_{tr}=10^2,10^3,\ldots,10^6$ (from bottom to top). Curves have been vertically shifted for clarity.

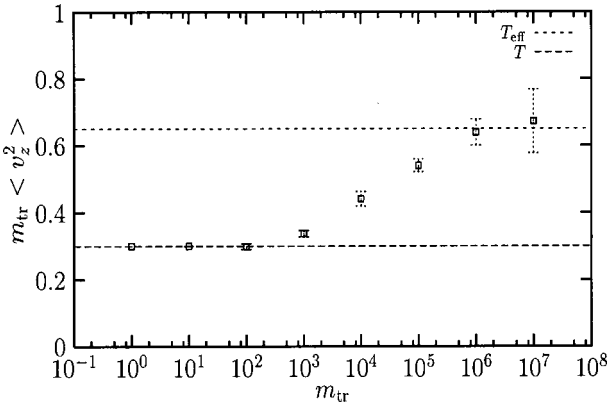

FIG. 20. Mass dependence of the mean kinetic energy in the z direction for $T=0.3$ and $\gamma=10^{-3}$. Horizontal lines are $T=0.3$ and $T_{eff}=0.65$. Error bars are evaluated from tracer to tracer fluctuations.

scale $t_s \sim t_{rel}$, then the Boltzmann weight for the subsystem will be given by $\exp(-E_s/T_{eff})$, with E_s the energy of the subsystem.[19] The thermometer does not measures the microscopic temperature, but the effective temperature associated with its characteristic time scale. In that sense, T_{eff} can correctly be described as an ''effective temperature.''

Here, we propose a concrete realization of this situation in which the thermometer is in fact a heavy particle, with a mass $m_{tr} \gg m$. Tuning the mass of the particle allows its Einstein frequency ω_E to be controlled, defined by[54]

$$\omega_E = \sqrt{\frac{\rho}{3m_{tr}} \int d^3\mathbf{r}\, g(r) \nabla^2 V(r)}, \tag{33}$$

which essentially characterizes the frequency of vibration for the particle in the cage formed by its neighbors. For particles of type A with $m_{tr}=1$, $\omega_E \tau_0 \simeq 20$ at $T=0.5$.

In our simulations, we have considered 10 massive tracer particles with masses in the range $m_{tr} \in [1,10^7]$. The tracer particles are otherwise identical to A particles, so that the equilibrium structure of the fluid is the same as with normal, ''light'' particles. Since the oscillation frequency is inversely proportional to the square root of the mass, the heaviest particles will have an Einstein frequency typically a thousand times smaller than the light ones, which puts their oscillation period in the range of typical relaxation times for the sheared supercooled fluid. Note that the Einstein frequency is entirely determined by static properties, and always determines the short time behavior of the velocity autocorrelation of the particle. Therefore it is a relevant quantity also for the description of heavy particles, moving in a fast environment.

Figure 19 compares the typical trajectories for heavy and light particles. The heavy particles are indeed seen to have a much lower oscillation frequency, and therefore their dynamics can be seen as involving a low-frequency filter coupled to the fluctuations of the host fluid, which corresponds to the slow, or ''effective thermometer'' considered in Ref. 19. In order to get the temperature from this thermometer, we compute the average mean square velocity in the direction transverse to the flow for these tracer particles. The results are shown in Fig. 20. From this figure, it is clear that light particles have a mean-squared velocity given by the usual bath temperature ($T=0.3$ in this case), which crosses over to the effective temperature $T_{eff}=0.65$ for the heaviest particles, $m_{tr} \sim 10^6 - 10^7$. Intermediate masses, $m_{tr} \sim 10^4 - 10^5$, corresponds to times scales located in the plateau region of the correlation which marks the crossover between equilibrium and off-equilibrium behaviors. This crossover is usually entirely hidden in the ''breaking points'' near the value $C_{\mathbf{k}} \sim q_k$ in previous parametric plots.

This implies that a *generalized equipartition theorem* holds for the heaviest tracers, with the effective temperature replacing the usual temperature, i.e.,

$$\left\langle \tfrac{1}{2} m_{tr} v_z^2 \right\rangle = \tfrac{1}{2} T_{eff}. \tag{34}$$

Moreover, we show in Fig. 21 that $P(v_z)$, the probability distribution of the velocity, is well approximated by a Gaussian shape,

$$P(v_z) = \sqrt{\frac{m_{tr}}{2\pi T_{eff}}} \exp\left[-\frac{m_{tr} v_z^2}{2 T_{eff}} \right]. \tag{35}$$

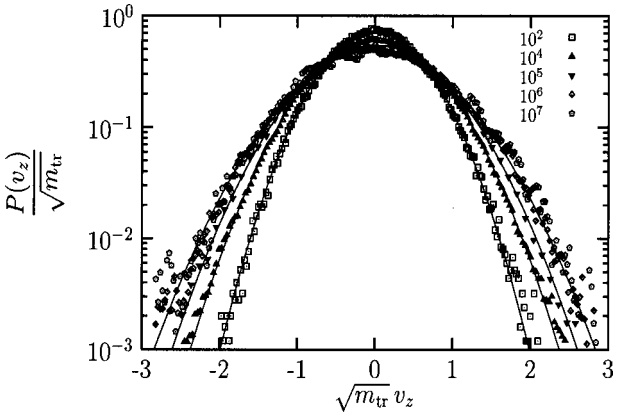

FIG. 21. Probability distribution function of the velocity v_z for various massive tracers, as indicating in the figure. The full lines are fits to the form (35) demonstrating the Gaussian shape for all the values of the mass investigated. Values of T_{eff} are $T_{eff}=0.3$ (equilibrium, $m_{tr}=10^2$), 0.44, 0.54 (crossover, $m_{tr}=10^4-10^5$), and 0.65 (asymptotic effective temperature, $m_{tr}=10^6-10^7$).

Downloaded 25 Jun 2007 to 128.135.152.55. Redistribution subject to AIP license or copyright, see http://jcp.aip.org/jcp/copyright.jsp

This in turn implies that the usual Maxwellian shape of the velocity distribution is recovered, again with $T_{\rm eff}$ replacing T.

The result, although expected on general grounds, is physically quite surprising. Again, it could be tested against experiments involving for instance colloidal particles, the tracers, in a complex fluid, e.g., polymeric. The important factor here is not the size of the tracer particle, but rather its mass that should be much larger than that of the fluid constituants.[55] One could also investigate the rotational degrees of freedom of nonspherical, ''slow'' tracer particles.

This result opens the way for new, simple determinations of effective temperatures in nonequilibrium glassy materials. Indeed, it has to be noted here that no ''complex'' dynamic functions such as correlations or susceptibilities are needed. This suggests that it would be extremely interesting to reproduce Perrin's experiment[56] on barometric equilibrium in a sheared colloidal suspension. Although we have not tested numerically this situation, we expect indeed that the barometric equilibrium of heavy particles inside a horizontally sheared fluid should also be ruled by the effective temperature of the fluid, higher than the room temperature.

IX. DISCUSSION

In this paper, we have investigated the correlation and response functions for a supercooled fluid undergoing steady shear flow. The ingredients essential to our study are the separation of time scales existing in the fluid at rest between the slow α relaxation and the microscopic times, and the energy input at large scales provided by the shear flow. With these minimal ingredients, it is possible to carry out a meaningful comparison with theoretical results obtained for this nonequilibrium dynamics at the mean-field, or schematic mode-coupling level. We also believe that the results should be of general relevance to many complex systems undergoing shear flow, for which the same ingredients are present.

We have first studied the nonlinear rheology of the system, which is indeed quite similar to what is observed in many complex systems. The system exhibits shear-thinning for shear rates exceeding the α-relaxation time. The results can be rescaled on a common curve as long as temperature remains higher than the critical mode-coupling temperature for this system. Below T_c, the shear-thinning behavior may alternatively be interpreted in terms of a temperature-dependent shear-thinning exponent, or a temperature-dependent yield stress. The fact that σ is nearly independent of the shear rate at low temperatures and shear rates makes the Lennard-Jones mixture a good candidate to study possible mechanical instabilities in Bingham fluids at a microscopic level.

In the shear flow, the system dynamics becomes stationary. This allows an accurate determination of the time-dependent correlation functions, as opposed to the case of aging systems, for which this determination is more difficult. We showed that several generic features of correlation functions observed in supercooled systems in the vicinity of T_c are still present out of equilibrium, as was predicted theoretically.[13] Among those, the two-step (β and α) relaxation, the stretching of the α relaxation and the factorization property that characterizes the spatial dependence in the β-relaxation regime.

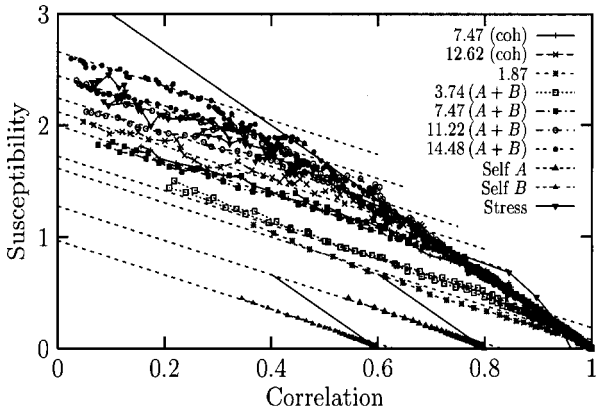

FIG. 22. Summary of our results for the effective temperature. We show here the 14 different susceptibility–correlation parametric plots described in the previous sections. They are all consistent with the same effective temperature for the slow modes. The full lines are the equilibrium FDT of slope $-1/0.3$; the dashed lines have slope $-1/0.65$.

Finally, we have investigated in great detail the violations of the fluctuation–dissipation theorem in this nonequilibrium system. Our results, which are summarized in a spectacular way in Fig. 22, are consistent with the expectation—based both on theoretical arguments and on earlier results from aging studies—that an effective temperature, independent of the observable under consideration, can be defined for the slow modes of the fluid. For several of the observables we considered, we suggested experimental probes that could be used to measure similar quantities in complex fluids.

We also presented a numerical realization of an ''effective thermometer'' that probes this effective temperature, using heavy tracer particles. The reading of the value of the effective thermometer follows from the generalization of the equipartition theorem to this nonequilibrium situation. This suggest a simple and elegant method to access the effective temperature. Again, we suggested experimental protocols that could realize these measurements.

It has to be noted that the notion of an effective (or fictive) temperature is a long-standing issue in the context of glassy materials (see, e.g., Ref. 1). However, our results clearly show that the definition Eq. (1) from a nonequilibrium fluctuation dissipation has all the properties that has to be captured by such a quantity.[19] (1) It is the temperature measured by a thermometer, and it includes naturally the separation of time scale of glassy systems, as shown by our ''tracer experiment.'' (2) It can be measured in a purely dynamic way, without making reference to any equilibrated, or extrapolated, state. (3) It is independent of the chosen observable, as we have clearly demonstrated. None of these points is satisfied by previous definitions of a fictive temperature.[1] Note that $T_{\rm eff}$ also captures the essential phenomenological idea that when a system is sheared more vigorously, its effective temperature increases. We thus emphasize here the huge physical interest of this quantity, well beyond the simple check of a sophisticated theoretical prediction.

Downloaded 25 Jun 2007 to 128.135.152.55. Redistribution subject to AIP license or copyright, see http://jcp.aip.org/jcp/copyright.jsp

All these results give strong support to the theoretical scenario elaborated from schematic mode-coupling theories to describe the rheology of soft glassy materials.[13] This shows that although these theories start from a rather crude description of a sheared fluid, they also capture its essential features. It is important to note that some of these features are present in no other theory, such as the emphasis put on the study of response functions, and the resulting FDT violations.

At the theoretical level, the next step to be performed is of course to give a more ''microscopic'' derivation of the nonequilibrium mode-coupling theory of Ref. 13 for the study of glassy materials under shear. In this respect, the results obtained by Latz[18] in its work on the aging regime are a very important step.

However, we believe that it now is time to perform systematic experiments to test quantitatively existing theories of the nonequilibrium dynamics of glassy materials. In that sense, the situation is more or less similar to the mid-1980s when schematic mode-coupling theories were already derived, but with little experimental confirmation of its main features. This is why we tried, as much as possible, to suggest experimental counterparts to our numerical measurements. We hope that our findings and suggestions in the present paper will motivate further experimental work in the field.

ACKNOWLEDGMENTS

It is a pleasure to thank Jorge Kurchan and Walter Kob for many useful discussions. This work was supported by the Pôle Scientifique de Modélisation Numérique at ENS-Lyon and the CDCSP at Université de Lyon. PSMN and CDCSP are supported by the Région Rhône-Alpes.

[1] R. G. Larson, *The Structure and Rheology of Complex Fluids* (Oxford University Press, New York, 1999).
[2] P. Sollich, F. Lequeux, P. Hébraud, and M. E. Cates, Phys. Rev. Lett. **78**, 2020 (1997); P. Sollich, Phys. Rev. E **58**, 738 (1998).
[3] L. C. E. Struik, *Physical Aging in Amorphous Polymers and other Materials* (Elsevier, Amsterdam, 1978).
[4] J.-Ph. Bouchaud, L. F. Cugliandolo, J. Kurchan, and M. Mézard, *Spin Glasses and Random Fields*, edited by A. P. Young (World Scientific, Singapore, 1998).
[5] L. Cipelletti, S. Manley, R. C. Ball, and D. A. Weitz, Phys. Rev. Lett. **84**, 2275 (2000).
[6] M. Cloitre, R. Borrega, and L. Leibler, Phys. Rev. Lett. **85**, 4819 (2000).
[7] L. Ramos and L. Cipelletti, Phys. Rev. Lett. **87**, 245503 (2001).
[8] M. Kroon, G. Wegdam, and R. Sprik, Phys. Rev. E **54**, 1 (1996); D. Bonn, H. Tanaka, G. Wegdam, H. Kellay, and J. Meunier, Europhys. Lett. **45**, 52 (1999); B. Abou, D. Bonn, and J. Meunier, Phys. Rev. E **64**, 021510 (2001).
[9] A. Knaebel, M. Bellour, J.-P. Munch, V. Viasnoff, F. Lequeux, and J. L. Harden, Europhys. Lett. **52**, 73 (2000).
[10] C. Dérec, A. Ajdari, and F. Lequeux, Faraday Discuss. **112**, 195 (1999); Eur. Phys. J. E **4**, 355 (2001).
[11] S. M. Clarke, F. Elias, and E. M. Terentjev, Eur. Phys. J. E **2**, 335 (2000).
[12] H. Horner, Z. Phys. B: Condens. Matter **100**, 243 (1996); L. F. Cugliandolo, J. Kurchan, P. Le Doussal, and L. Peliti, Phys. Rev. Lett. **78**, 350 (1997); F. Thalmann, Eur. Phys. J. B **19**, 49 (2001); **19**, 65 (2001).
[13] L. Berthier, J.-L. Barrat, and J. Kurchan, Phys. Rev. E **61**, 5464 (2000).
[14] U. Bengtzelius, W. Götze, and A. Sjölander, J. Phys. C **17**, 5915 (1984); E. Leutheusser, Phys. Rev. A **29**, 2765 (1984).
[15] T. R. Kirkpatrick and P. G. Wolynes, Phys. Rev. A **35**, 3072 (1987); T. R. Kirkpatrick and D. Thirumalai, Phys. Rev. B **36**, 5388 (1987).
[16] W. Götze, in *Liquids, Freezing and Glass Transition*, edited by J. P. Hansen, D. Levesque, and J. Zinn-Justin (North-Holland, Amsterdam, 1991); W. Götze and L. Sjögren, Rep. Prog. Phys. **55**, 241 (1992); W. Götze, J. Phys.: Condens. Matter **11**, A1 (1999).
[17] J.-P. Bouchaud, L. F. Cugliandolo, J. Kurchan, and M. Mézard, Physica A **226**, 243 (1996).
[18] A. Latz, J. Phys.: Condens. Matter **12**, 6353 (2000); e-print cond-mat/0106086.
[19] L. F. Cugliandolo, J. Kurchan, and L. Peliti, Phys. Rev. E **55**, 3898 (1997).
[20] L. F. Cugliandolo and J. Kurchan, Phys. Rev. Lett. **71**, 173 (1993).
[21] R. Yamamoto and A. Onuki, Europhys. Lett. **40**, 61 (1997); Phys. Rev. E **58**, 3515 (1998).
[22] A. J. Liu and S. R. Nagel, Nature (London) **396**, 21 (1998).
[23] S. A. Langer and A. J. Liu, Europhys. Lett. **49**, 68 (2000); I. K. Ono, C. S. O'Hern, S. A. Langer, A. J. Liu, and S. R. Nagel, e-print cond-mat/0110276.
[24] P. Hébraud and F. Lequeux, Phys. Rev. Lett. **78**, 4657 (1997).
[25] L. F. Cugliandolo, J. Kurchan, and P. Le Doussal, Phys. Rev. Lett. **76**, 2390 (1996).
[26] L. F. Cugliandolo and J. Kurchan, Physica A **263**, 242 (1999); J. Phys. Soc. Jpn. **69**, 247 (2000).
[27] S. Fielding and P. Sollich, Phys. Rev. Lett. **88**, 050603 (2002).
[28] W. Kob and H. C. Andersen, Phys. Rev. E **52**, 4134 (1995); **51**, 4626 (1995); Phys. Rev. Lett. **73**, 1376 (1994).
[29] Note that in previous works (Refs. 28 and 30) a different time unit, $\tau = (m_A \sigma_{AA}^2 / 48 \varepsilon_{AA})^{1/2}$, is often used when dealing with Lennard-Jones particles.
[30] W. Kob and J.-L. Barrat, Phys. Rev. Lett. **78**, 4581 (1997); Europhys. Lett. **46**, 637 (1999); Eur. Phys. J. B **13**, 319 (2000).
[31] D. J. Evans and G. Morriss, *Statistical Mechanics of Nonequilibrium Liquids* (Academic, London, 1990); http://rsc.anu.edu.au/~evans/evansmorrissbook.htm
[32] M. Allen and D. Tildesley, *Computer Simulation of Liquids* (Oxford University Press, Oxford, 1987).
[33] Strictly speaking, it is not impossible to observe inhomogeneous flow under such conditions, see, e.g., Ref. 34; such instabilities, however, seem to correspond to inverse shear rates of the order of microscopic oscillation times, higher than those we are using.
[34] M. Stevens and M. O. Robbins, Phys. Rev. E **48**, 3778 (1993).
[35] As discussed in Ref. 34, potential problems implying various thermostats are expected only in fluid systems where the shear rate is such that a particle moves by an appreciable fraction of its diameter on a phonon period. In our simulation, even the larger shear rate is ($\gamma = 0.1$) is not in this range.
[36] J. D. Ferry, *Viscoelatic Properties of Polymers* (Wiley, New York, 1980).
[37] M. O. Robbins and M. H. Müser, in *Handbook of Modern Tribology*, edited by B. Bhushan (CRC, Boca Raton, 2001); e-print cond-mat/0001056.
[38] V. Trappe, V. Prasad, L. Cipelletti, P. N. Segre, and D. A. Weitz, Nature (London) **411**, 772 (2001).
[39] M. D. Ediger, C. A. Angell, and S. R. Nagel, J. Phys. Chem. **100**, 13200 (1996).
[40] D. M. Heyes, J. J. Kim, C. J. Montrose, and T. A. Litovitz, J. Chem. Phys. **73**, 3987 (1980).
[41] L. F. Cugliandolo and G. Lozano, Phys. Rev. Lett. **80**, 4979 (1998).
[42] L. Berthier, L. F. Cugliandolo, and J. L. Iguain, Phys. Rev. E **63**, 051302 (2001).
[43] J.-L. Barrat and L. Berthier, Phys. Rev. E **63**, 012503 (2001).
[44] T. S. Grigera and N. E. Israeloff, Phys. Rev. Lett. **83**, 5038 (1999).
[45] L. Bellon, S. Ciliberto, and C. Laroche, Europhys. Lett. **53**, 511 (2001); L. Bellon and S. Ciliberto, Physica D, cond-mat/0201224.
[46] L. Bellon, Ph.D. thesis, Ecole Normale Supérieure de Lyon (2001).
[47] D. Hérissonr and M. Ocio, cond-mat/0112378.
[48] J.-P. Bouchaud, in *Soft and Fragile Matter, Nonequilibrium Dynamics, Metastability and Flow*, edited by M. E. Cates and M. R. Evans (Institute of Physics, Bristol, 2000); e-print cond-mat/9910387.
[49] See, e.g., P. Pusey, in *Liquids, Freezing and Glass Transition*, edited by J. P. Hansen, D. Levesque, and J. Zinn-Justin (North-Holland, Amsterdam, 1991).
[50] G. Parisi, Phys. Rev. Lett. **79**, 3660 (1997).
[51] R. Di Leonardo, L. Angelani, G. Parisi, and G. Ruocco, Phys. Rev. Lett. **84**, 6054 (2000).
[52] M. Sellitto, Eur. Phys. J. B **4**, 135 (1998).
[53] H. Makse and J. Kurchan, Nature (London) **415**, 614 (2002).

Downloaded 25 Jun 2007 to 128.135.152.55. Redistribution subject to AIP license or copyright, see http://jcp.aip.org/jcp/copyright.jsp

[54] J. P. Hansen and I. R. McDonald, *Theory of Simple Liquids*, 2nd ed. (Academic, London, 1986).
[55] Obviously, it is not possible to achieve experimentally the situation of large mass and small tracer size. Our goal here was to realize in the simplest possible way a ''slow'' degree of freedom. As indicated in the discussion, we expect that the important word here is ''slow.'' Actual tracers (Brownian particles), which are also ''large'' particles, are expected to feel the slow components of the fluid motion essentially in the same way as the small, heavy tracers we are considering.
[56] J. Perrin, Ann. Chim. Phys. **18**, 1 (1909).

Downloaded 25 Jun 2007 to 128.135.152.55. Redistribution subject to AIP license or copyright, see http://jcp.aip.org/jcp/copyright.jsp